Brief Communication

MOLECULAR METABOLISM

GLP-1R signaling does not modify the severity of experimental graft versus host disease

Bernardo Yusta, Chi Kin Wong, Dianne Matthews, Jacqueline A. Koehler, Laurie L. Baggio, KW Annie Bang, Daniel J. Drucker*

ABSTRACT

Objective: Glucagon-like peptide-1 (GLP-1) reduces systemic and gut inflammation. Here we assessed whether gain or loss of GLP-1 receptor (GLP-1R) signaling modifies the extent of gut injury and inflammation in experimental murine acute graft vs. host disease (aGvHD).
Methods: Allogeneic hematopoietic cell transplantation (HCT) was performed using bone marrow and splenocytes from BALB/c donors to induce aGvHD in C57BL/6 recipients or vice versa. Chimerism was determined by flow cytometry analysis of immune cell compartments. Inflammation was assessed by histological scoring of gut mucosal damage and by measuring circulating cytokine levels. qPCR was used to quantify gene expression in small intestine immune cells and tissues. The gut microbiome was assessed by 16S rRNA sequencing.
Results: Allogeneic chimerism was greater than 90% in peripheral blood and in the gut epithelial compartment. Levels of *Glp1r* mRNA transcripts were induced in the ileum of both vehicle- and semaglutide-treated allogeneic mice, reflecting that allogeneic T cells homing to the gut express a functional GLP-1R. Nevertheless, semaglutide did not attenuate the severity of systemic cytokine induction, gut injury or inflammation, or the extent of aGvHD in the gut mucosa. Loss of GLP-1R signaling in donor cells had limited effects on overall microbial diversity during acute GvHD, and semaglutide-treated mice exhibited modest changes in proportions of microbial species.
Conclusions: Although gut T cells express a functional GLP-1R, GLP-1R signaling has no meaningful impact on systemic or intestinal inflammation or microbiota composition in mice with experimental aGvHD, highlighting that the anti-inflammatory actions of GLP-1 medicines are highly context-dependent.

Keywords Gut; Inflammation; T cells; GPCR; Microbiota; Glucagon-like peptides

1. INTRODUCTION

Glucagon-like peptides, exemplified by glucagon-like peptide-1 (GLP-1) and glucagon-like peptide-2 (GLP-2) are produced in the brain and in the distal gut, and regulate energy intake and glucose homeostasis. The metabolic actions of GLP-1 are conserved in people living with type 2 diabetes (T2D) and obesity, supporting development of multiple GLP-1 medicines for the treatment of T2D and for weight loss in people with overweight or obesity [1]. Both GLP-1 and GLP-2 also exert direct actions on the gut to control gut motility and reduce gut inflammation [2,3].
Initial studies of GLP-1 biology centered on its role in regulating islet hormone secretion and glucose homeostasis. Subsequent experiments revealed mechanisms and cell types in the brain that contribute to regulating energy intake [4]. More recently, the enteroendocrine L cell has been shown to act as an inflammation sensor in animals and humans, secreting GLP-1 and GLP-2 in response to gut injury and inflammation arising from infectious or non-microbial sources [5—8]. GLP-1 also exerts direct and indirect actions to preserve gut health, including induction of small bowel growth via stimulation of crypt fission [9,10]. Both GLP-1 and GLP-2 preserve gut integrity and reduce mucosal damage in preclinical studies of experimental gut injury [11—16]. The actions of GLP-2 on the gut epithelium are partially indirect, acting on enteric neurons and populations of subepithelial myofibroblasts to maintain barrier function, expand the mucosal epithelium, and reduce local gut inflammation [17].
GLP-1 acts on cellular targets distinct from those mediating GLP-2 action to improve gut barrier function and attenuate gut inflammation [18,19]. Anti-inflammatory actions of GLP-1 in the gut have been localized to group 3 innate lymphoid cells (ILC3s) in mice, as liraglutide induced ILC3-dependent cytokines in mice with experimental colitis, and the protective effect of liraglutide on gut histology and immune cell infiltration was abrogated in ILC3-deficient RORgt$^{gfp/gfp}$ mice with dextran sodium sulfate (DSS)-induced colitis [15]. Within the proximal regions of the gut, Brunner's glands in the duodenum express high levels of the GLP-1 receptor (GLP-1R) and acute administration of the GLP-1R agonist (GLP-1RA) exendin-4 upregulates the expression of mRNAs for *Muc5b, Muc5ac, Gcnt1*, and *Il33* in murine Brunner's glands, findings replicated in separate studies using acute administration of liraglutide [13]. Consistent with findings from these gene expression analyses, semaglutide directly stimulates mucus secretion from Brunner's glands, contributing to the augmentation of barrier function and protection of absorptive enterocytes [20].
GLP-1 also reduces local gut inflammation through actions on subsets of intestinal intraepithelial lymphocytes (IELs) residing within the small

From the Lunenfeld Tanenbaum Research Institute, Mt. Sinai Hospital, Toronto, ON M5G1X7, Canada

*Corresponding author. Mt. Sinai Hospital, LTRI, 600 University Avenue Mailbox39, Toronto, ON M5G 1X7, Canada. E-mail: drucker@lunenfeld.ca (D.J. Drucker).

Received July 20, 2025 • Revision received August 6, 2025 • Accepted August 13, 2025 • Available online 20 August 2025

https://doi.org/10.1016/j.molmet.2025.102235

bowel mucosa adjacent to GLP-1 secreting L cells. IELs express high levels of the canonical GLP-1R and the GLP-1RA exendin-4 acutely induces cyclic AMP accumulation and downregulates cytokine production from activated IELs ex vivo [12]. Consistent with an anti-inflammatory role for endogenous GLP-1, *Glp1r*$^{-/-}$ mice exhibit dysbiosis, dysregulation of inflammation-related mRNA transcripts in the small bowel, and enhanced sensitivity to mucosal injury following exposure to DSS [12]. Remarkably, bone marrow transplantation from *Glp1r*$^{+/+}$ mice to restore GLP-1R + immune cells in the gut of *Glp1r*$^{-/-}$ mice normalized expression of genes regulating immune function and epithelial integrity that were dysregulated in the gut of *Glp1r*$^{-/-}$ mice [12].

The emerging literature linking GLP-1R signalling to control of immune-mediated tissue injury is supported by studies demonstrating that augmentation of GLP-1R signalling prolonged heart and islet survival and delayed allograft rejection in mice, effects associated with reduced immune cell infiltration in transplanted heart and islets [21]. Conversely transplantation of *Glp1r*$^{-/-}$ T cells conferred greater allograft rejection and a heightened immune response in mice following heart transplantation. Consistent with these findings, activation of GLP-1R signalling reduced the extent of immune cell infiltration, fibrosis and allograft rejection in mice following cardiac transplantation; similar findings were observed in rats treated with the GLP-1R/GCGR dual agonist TB001 following kidney transplantation [22,23].

Accumulating evidence demonstrates the widespread anti-inflammatory activity of GLP-1 medicines in multiple organs in both preclinical and clinical studies [24,25]. Intriguingly, higher circulating levels of GLP-1 were associated with a reduced risk of acute graft-versus-host disease (aGvHD) in patients undergoing allogeneic hematopoietic stem cell transplantation (HSCT) [26]. These findings have spurred the initiation of a clinical trial to test the efficacy of semaglutide administration in patients with lymphoma at risk for gastrointestinal mucositis during treatment with chemotherapy and HSCT [27]. Here we examined the consequences of gain vs. loss of GLP-1R signaling in mice with aGvHD, a disorder characterized by a systemic inflammatory syndrome, often presenting clinically with severe intestinal inflammation and gut tissue damage. Surprisingly, augmentation of GLP-1R signaling with semaglutide or genetic disruption of GLP-1R signaling in donor cells transplanted into allogeneic recipients, failed to reduce inflammation or the extent of gut mucosal injury, and produced only modest changes in gut microbiota profiles in a well-established murine model of aGvHD.

2. MATERIALS AND METHODS

2.1. Mice

Wild-type (WT) BALB/c (H-2^{d}) and C57BL/6 (H-2^{b}) mice were from The Jackson Laboratory. Whole-body *Glp1r*$^{-/-}$ mice [28] and *Glp1r*$^{+/+}$ control mice were generated by crossing *Glp1r*$^{+/-}$ mice on the C57BL/6 genetic background in the specific pathogen-free colony at the Toronto Centre for Phenogenomics (Mt. Sinai Hospital, Toronto, ON, Canada). All experiments were performed in mice housed up to five per cage, maintained on a 12-h light/dark cycle with free access to standard rodent chow (18% kcal from fat) (Teklad global) and acidified drinking water. All experiments were conducted according to protocols approved by the Animal Care and Use Subcommittee at the Toronto Centre for Phenogenomics and were consistent with Animal Research: Reporting In Vivo Experiments guidelines.

2.2. Hematopoietic cell transplantation (HCT)

Mouse bone marrow cells were isolated from femurs and tibiae, and splenocytes from the same donors were used as a source of T cells. Cell suspensions were prepared in DMEM:F12 media with penicillin/streptomycin, subjected to red blood cell (RBC) lysis, and counted using a hemocytometer. The murine acute GvHD (aGvHD) model used in these experiments involved Major Histocompatibility Complex (MHC)-fully mismatched transplants between male donor and recipient pairs. Mice were 8—10 weeks of age at the time of transplantation. Recipient mice were lethally irradiated (C57BL/6 were given a total of 1,100 cGy and BALB/c a total of 850 cGy, split into two equal doses 4 h apart) using a Gammacell 40 instrument as described [12,29,30] and subsequently reconstituted via tail vein injection. C57BL/6 recipients of allogeneic BALB/c donors received 5x10^{6} bone marrow cells and 10-15x10^{6} splenocytes; BALB/c recipients of allogeneic C57BL/6 donors received 5x10^{6} bone marrow cells and 0.25x10^{6} splenocytes. Transplantation with cells from syngeneic donors, which lack an alloreactive immune response, was used as a negative control. No antibiotic treatment was utilized in the context of the HCTs. To minimize potential 'cage effects,' bedding from all mouse cages involved in the experiments was regularly mixed both before and after HCT. Mice were monitored daily and euthanized when they had lost $\geq$20% of their pre-transplantation body weight. The day of euthanasia was considered as the date of death for survival studies. Donor chimerism was assessed at sacrifice by flow cytometry on peripheral blood mononuclear cells (PBMC) and on the epithelial compartment and neighboring associated immune cells (ECI) isolated from the small intestine.

2.3. Peptides and treatments

The GLP-1RAs semaglutide and exendin-4 were from Novo Nordisk Inc and Chi Scientific Inc, respectively. Peptide stocks were diluted in phosphate buffered saline (PBS) without calcium or magnesium (vehicle). Semaglutide was administered to mice by subcutaneous injection at a dose of 10 μg/kg once daily, a relatively low dose chosen to minimize weight loss while maintaining high efficacy in controlling glucose homeostasis and attenuating experimental inflammation and atherosclerosis in mice [31,32].

2.4. Tissue collection and processing

Following euthanasia, the small intestine from the pyloric sphincter to the ileocecal junction was resected, cleaned of mesenteric fat, and divided into quarters. The first and third quarters were used to isolate the epithelial compartment and ECI. Sampling outwards from the ileocecal junction, adjacent 2-cm segments were collected from the ileum. Ileal tissue samples were fixed in 10% neutral-buffered formalin at room temperature for 24 h, then processed and embedded in paraffin blocks, or snap-frozen in liquid nitrogen and stored at −80 °C for later RNA extraction.

2.5. Intestinal histomorphometry

Paraffin sections (4 μm thick) were stained for hematoxylin-eosin (H&E) using a Sakura Finetek Tissue-Tek Prisma® *Plus* Automated Slide Stainer. For each mouse, a minimum of 20 well-oriented crypts were selected from at least 4—5 different ileal cross-sections. The numbers of Paneth cells (identified by their eosinophilic granules) per crypt and apoptotic bodies per crypt were scored in a blinded manner. Representative digital histological images were acquired using a Leica DMR microscope equipped with a Leica DC300F camera and Leica Qwin V3 software.

2.6. Isolation of small intestine immune cells

After flushing the luminal contents with PBS, the first and third small intestine segments (as described above) were opened longitudinally

and cut into small pieces. The tissue was then incubated in 5 mM ethylenediaminetetraacetic acid (EDTA), 1 mM dithiothreitol (DTT) and 10 mM HEPES in Hank's Balanced Salt Solution (HBSS) without calcium or magnesium at 37 °C for 15 min in a shaker incubator and then subjected to multiple rounds of vortexing at full power for 30 s to fully strip the epithelial compartment and ECI. Tissue fragments were removed by sequential filtering through a 500 μm strainer followed by a 100 μm strainer. The final suspension was centrifuged to pellet the cells, which were then resuspended in 44% Percoll in RPMI 1640 media at 22 °C and centrifuged at 700×*g* for 20 min. The pellet was washed and processed for flow cytometry and RNA analysis. Alternatively, for fluorescence-activated cell sorting (FACS) analysis, the pellet obtained after sequential filtration through 500 μm and 100 μm strainers was resuspended in 44% Percoll in RPMI 1640 at 22 °C and layered over a 67% Percoll in RPMI 1640 solution. The Percoll gradient was centrifuged at 700×*g* for 20 min without acceleration or braking. The interphase was recovered, washed, and the resulting cell pellet was used for FACS.

Immune cells from the conjoined intestinal lamina propria, submucosa and muscle layers (referred to collectively as LPM) were isolated following a published protocol [33]. The entire small intestine was cleared of luminal contents, opened longitudinally, and cut into small pieces. The intestinal fragments were then incubated in 5 mM EDTA, 5 mM DTT, and 2% v/v fetal bovine serum (FBS) in HBSS without calcium or magnesium (buffer A) in a shaker incubator at 37 °C for 15 min to strip the epithelial compartment. The gut tissue pieces were vortexed briefly and the supernatant was discarded. After four rounds of 15 min washes in buffer A at 37 °C, the tissues were minced and transferred into 10 mM HEPES in HBSS. DNase I 200 KU/mL and Liberase TM 0.2 Wünsch U/mL were added and the tissues were incubated at 37 °C for 30 min. After stopping the digestion with 0.5 mL FBS the tissues were gently triturated into single cell suspensions, filtered through a 40 μm strainer, spun down to pellet the cells and then subjected to a 44%/67% Percoll gradient as indicated above prior to processing for FACS.

2.7. Flow cytometry and fluorescence-activated cell sorting (FACS)

Samples were first treated with anti-mouse CD16/CD32 antibody (Fc block) prior to incubation for 20 min at 4 °C with cell surface marker anti-mouse antibodies (see Supplementary Methods), in parallel with the corresponding compensation and staining controls. The viability marker 4′,6-diamidino-2-phenylindole (DAPI) was included to discriminate live cells. For identification and FACS of small intestine ECI T cells, we used antibodies against the following antigens: H-2^{d} or H-2^{b} for BALB/c or C57BL/6 grafts, respectively, CD45.2, CD3, CD8a, CD69 and CD103. For identification and FACS of intestinal LPM T cells we used: H-2^{d}, CD45.2, CD3 and CD8a. For analysis of PBMC we used H-2^{d} or H-2^{b} for BALB/c or C57BL/6 grafts, respectively, CD45.2, CD3 and CD8a. Stained cells were analyzed on a Gallios flow cytometer and FACS enrichment was performed on a MoFlo Astrios cell sorter, both instruments from Beckman Coulter.

2.8. RNA extraction, cDNA synthesis, and PCR

Total RNA was extracted from mouse tissues or from FACS sorted cells by the guanidinium thiocyanate method using TRI Reagent. Reverse transcription (RT) was performed in RNA samples treated with DNase I, using random hexamers and SuperScript III. The resulting cDNA was used for both conventional and for real-time qPCR. PCR amplification of the murine *Glp1r* was accomplished as described [34] using Platinum *Taq* DNA polymerase and primers that amplify a 1.4-kb product encompassing the majority of the *Glp1r* open reading frame. Glyceraldehyde-3-phosphate dehydrogenase (*Gapdh*) PCR amplification was performed as described [35]. PCR products were analyzed by agarose gel electrophoresis using SYBR Safe DNA Gel Stain. Real-time qPCR was performed on a QuantStudio 5 System from Thermo Fisher Scientific with TaqMan Fast Advanced Master Mix and TaqMan Gene Expression Assays (Supplementary Methods). Relative quantification of transcript levels in whole intestine samples was performed using the comparative cycle threshold (Ct) method, with *Rpl32* or *Ppia* as endogenous normalization controls. Transcript abundance was reported as raw Ct values in cases where samples exhibited intrinsic expression differences relative to the RNA transcripts commonly used for normalization.

2.9. Plasma cytokine analysis

Plasma concentrations of TNFα, IL-10, IL-12 p70, IL-1β, IL-6, CXCL1, IFNγ, IL-2, IL-4 and IL-5, were measured in samples of heparinized cardiac blood using the V-PLEX Proinflammatory Panel 1 Mouse Kit from Meso Scale Discovery as per the manufacturer's instructions.

2.10. cAMP assay

cAMP concentrations were analysed in FACS sorted T cells from small intestine ECI using the acetylated version of the Direct cAMP ELISA Kit from Enzo Life Sciences as per manufacturer's instructions. After a 30—40 min post-sorting recovery period at 37 °C in RPMI 1640 with 10% FBS and 5 μM 2-mercaptoethanol, the cell suspension was centrifuged and the pellet resuspended in HBSS containing 5 mM HEPES, 0.1% Bovine Serum Albumin (BSA) and 300 μM 3-isobutyl-1-methylxanthine (IBMX) at 37 °C prior to agonist testing using 0.5—0.8 x10^{6} cells per assay. Forskolin (Fk) was used as a positive control.

2.11. 16S rRNA-seq analysis

Microbiota profiling was conducted via 16S rRNA gene sequencing, following methods previously described [11]. Fecal material was harvested from the distal colon, and genomic DNA was isolated for amplification of the V3—V4 hypervariable regions of the 16S rRNA gene. Amplicons were barcoded and prepared into sequencing libraries, which were subsequently run on an Illumina MiSeq platform using 2 × 300 bp paired-end reads. Raw sequence data underwent adaptor removal and quality filtering prior to denoising and taxonomic classification using the DADA2 pipeline [36]. Downstream processing was performed with the phyloseq package [37], and differential abundance was assessed using both DESeq2 [38] and LEfSe [39]. Predicted functional pathway analyses were conducted using PICRUSt2 [40].

2.12. Statistical analysis

Data are expressed as mean ± SD. As indicated in the Figure Legends, Student's t-tests and 1- or 2-way ordinary ANOVA followed by the appropriate post-hoc tests were used to calculate statistical significance. Survival curves were plotted using Kaplan—Meier estimates and compared using the Mantel—Cox log-rank test. Statistical analyses and graph generation were performed using Prism 10 software from GraphPad.

3. RESULTS

MHC-fully mismatched allogeneic HCT from BALB/c donors into C57BL/6 recipients, or vice versa, induces robust T cell-mediated aGvHD, with tissue pathology typically manifesting in the intestines within 10 days post-transplantation [41,42]. As illustrated in the

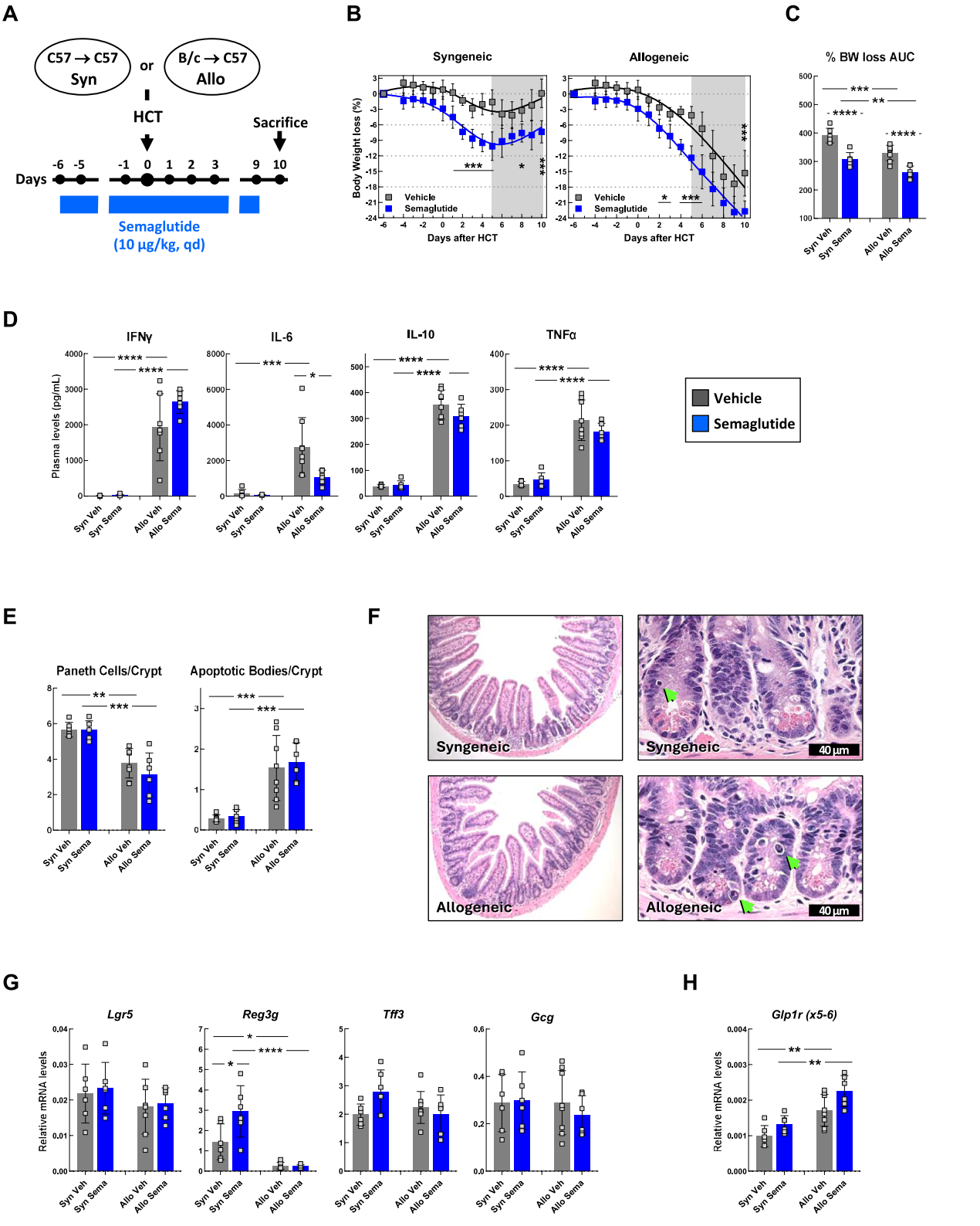

experimental design (Figure 1A), mice were treated with semaglutide or vehicle for 6 days before undergoing HCT, and treatment continued until sacrifice. Consistent with the established anorectic effects of GLP-1RAs, semaglutide induced a modest reduction in body weight (3.6%) before HCT. Myeloablative total body irradiation (TBI) was administered as pre-transplant conditioning, followed by allogeneic HCT using bone marrow and splenocytes (as source of T cells) from BALB/c donors to induce aGvHD in the gastrointestinal (GI) tract. In parallel, a separate set of transplants using syngeneic C57BL/6 donors was performed to generate aGvHD-negative controls, which received the same pre-transplant conditioning without the subsequent alloreactive immune response. Radiation injury led to predictable body weight (BW) loss in both the syngeneic and allogeneic groups during the first 5 days after HCT, which was more pronounced in the semaglutide-treated mice (Figure 1B). Subsequently, and independent of treatment, the syngeneic-transplanted mice started to regain BW whereas the BW of the allogeneic-transplanted mice continued to decline (grey shaded area in Figure 1B). As shown in Figure 1C, which depicts the %BW loss area under the curve (AUC) over the course of the experiment, allogeneic-transplanted mice exhibited greater BW loss compared to the syngeneic group, consistent with more active aGvHD. BW loss was greater with semaglutide in both syngeneic- and allogeneic-transplanted mice.

In the allogeneic transplantation-HCT setting, the myeloablative TBI procedure and the activated immune system from the donor synergize to inflict damage on the transplant recipient's GI tract, leading to loss of mucosal barrier function and the translocation of endotoxin [43]. This results in widespread tissue cytokine release and the systemic "cytokine storm" characteristic of aGvHD [44,45]. Circulating levels of typical proinflammatory cytokines IFNγ, IL-6, IL-10 and TNFα were markedly induced in the plasma of the allogeneic-transplanted mice compared to the syngeneic-transplanted group (Figure 1D). Although semaglutide administration reduced circulating levels of IL-6, levels of IFNγ, IL-10, and TNFα were not different in semaglutide-treated mice after allogeneic transplantation (Figure 1D).

The GI tract is a major initial aGvHD target organ [46,47]. Early after transplantation, allogeneic activated donor T cells migrate to the intestine and preferentially invade the lower crypt region lamina propria [41]. To assess the recruitment of allogeneic BALB/c T cells to the gut, we stripped the epithelial compartment and neighbouring associated immune cells (ECI) with a buffer containing 5 mM EDTA and performed flow cytometry with cell surface marker anti-mouse antibodies. As shown in Supp. Figure 1, allogeneic BALB/c chimerism was greater than 90% both in peripheral blood mononuclear cells (PBMC) (Supp. Fig. 1A) and the ECI (Supp. Figure 1B left panel) and not different between vehicle- vs. semaglutide-treated mice. Within the ECI, the percentage of allogeneic BALB/c CD3+CD8a+ T cells was similar in vehicle- and semaglutide-treated mice (70–75% of the CD45+ events) (Supp. Figure 1B middle panel). Most of those allogeneic T cells were CD69+ and a small fraction were CD69+ CD103+ (Supp. Figure 1B middle panel), contrasting with the >90% double positive CD69+ CD103+ tissue retention phenotype [48] characteristic of the residual IEL T cells (~5%) from the C57BL/6 host (Supp. Figure 1B right panel).

Tissue injury to the intestinal crypt epithelium is a characteristic finding of GvHD in transplant recipients. The crypts contain the stem cells and progenitors of the intestinal epithelium and in mice with GvHD, both Intestinal Stem Cells (ISCs) and Paneth cells are reduced as they undergo apoptosis mediated by pathogenic donor T cell-derived IFNγ [49]. We determined the extent of intestinal crypt damage by scoring the number of Paneth cells (identified by their eosinophilic granules) and apoptotic bodies/crypt in H&E-stained histological ileum sections. As quantified in Figure 1E and illustrated in representative images in Figure 1F, compared to syngeneic mice, there was a reduction in the number of Paneth cells/crypt and a concurrent increase of apoptotic bodies/crypt in the allogeneic group, consistent with the demise of crypt epithelial cells. No difference related to treatment (vehicle or semaglutide) was observed in either the syngeneic or allogeneic groups.

Levels of mRNA biomarkers in the ileum for the ISC compartment such as *Lgr5* and some epithelial secretory cell lineages (*Tff3* and *Gcg*) were not different between syngeneic and allogeneic-transplanted mice and no differences were observed in either vehicle- vs. semaglutide-treated mice (Figure 1G). In contrast, the mRNA expression of the aGvHD biomarker *Reg3g,* produced by multiple epithelial lineages [50], was induced by semaglutide in syngeneic mice yet suppressed in allogeneic mice irrespective of treatment (Figure 1G). Surprisingly, compared to the syngeneic group, levels of *Glp1r* mRNA transcripts were induced in the ileum of both vehicle- and semaglutide-treated allogeneic mice (Figure 1H). In the GI tract, the GLP-1R is expressed in enteric neurons and IELs [12,51,52]. The *Glp1r* from the host enteric neurons could contribute to ileal *Glp1r* expression observed in mRNA from allogeneic mice, but that wouldn't be expected for the IELs since the ECI from allogeneic mice only contains a minor fraction (~5%) of host *Glp1r* expressing IELs (Supp. Figure 1B left panel).

To investigate the source and potential importance of the unanticipated induction of *Glp1r* expression in the ileum of allogeneic mice, a BALB/c-into-C57BL/6 MHC-mismatched allogeneic-HCT was performed (Figure 2A). Immune cells from the LPM and ECI were isolated from transplant recipients on days 9 and 10 post-transplant and then analyzed by FACS. qPCR was used to examine relevant gene expression markers in the sorted allogeneic T cell populations. As a reference control, we also isolated ECI from WT C57BL/6 mice and sorted their corresponding T cells.

Allogeneic BALB/c chimerism was 95% in PBMC, 99% in the ECI, and 83% in LPM. Normal WT ECI largely consisted of CD8a+ T cells; in contrast, allogeneic ECI and LPM contained a sizeable percentage of both CD8a+ and CD8a- T cells (Figure 2B). Upon qPCR analysis, we unexpectedly found that allogeneic CD8a+ T cells sorted from the intestinal ECI expressed *Glp1r* mRNA at levels equivalent to those detected in RNA from typical sorted WT ECI T cells (Figure 2C).

Figure 1: Chronic semaglutide treatment does not reduce gut tissue damage or the typical features of aGvHD. (A) Schematic of the experimental design. Following a 6-day pretreatment period with vehicle (Veh) or semaglutide (Sema), C57BL/6 (C57) mice underwent HCT from syngeneic (Syn) C57BL/6 donors (n = 6 Veh and 6 Sema pretreated) or allogeneic (Allo) BALB/c (B/c) donors (n = 8 Veh and 8 Sema pretreated) and continued with the same Veh or Sema treatment regimen until the time of sacrifice. **(B and C)** (B) Sequence of body weight (BW) loss and (C) Area under the curve (AUC) of BW loss during the experiment. The grey shaded area in panel (B) is a visual reference to compare the body weight decline in the allogeneic mice relative to the syngeneic group indicative of the aGvHD progress. **(D)** Plasma cytokine levels. **(E)** Number of Paneth cells and apoptotic bodies/crypt in ileal tissue. **(F)** Representative histological sections of ileum stained with H&E. Arrowheads indicate apoptotic epithelial cells within the crypt compartment. **(G)** mRNA expression of select epithelial cell lineage markers and **(H)** *Glp1r* in ileum measured by qPCR. Data are mean ± SD pooled from 2 independent experiments comprising mice from the same cohort. *$p \leq 0.05$, **$p \leq 0.01$, ***$p \leq 0.001$ and ****$p \leq 0.0001$ by 2-way ANOVA followed by Sidak's (panel **B**) or Tukey's (panels **C** to **E**, **G** and **H**) multiple comparisons tests.

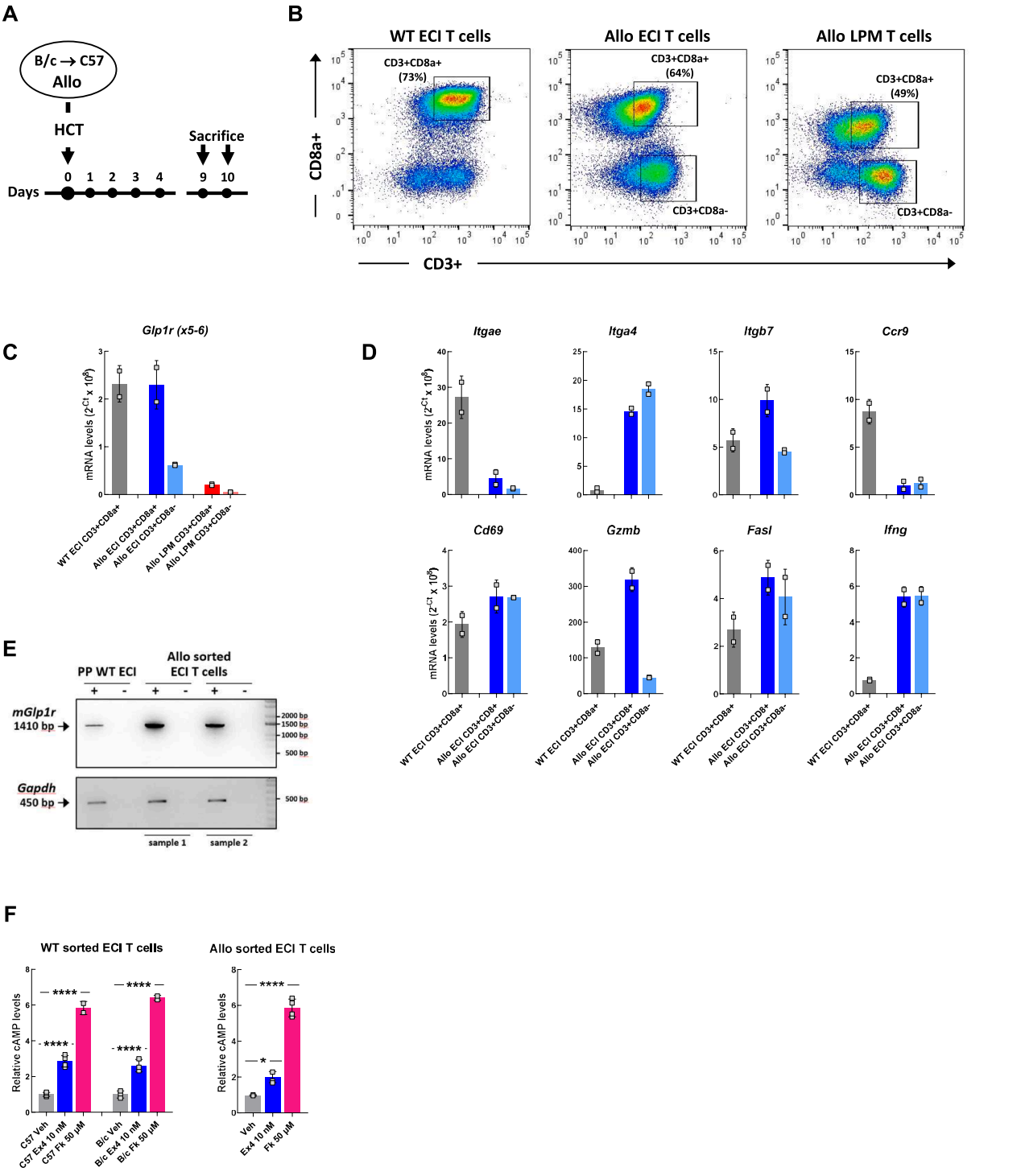

Allogeneic ECI CD8a- T cells, as well as allogeneic LPM T cells, also expressed *Glp1r* mRNA but at a lower level than sorted allogeneic ECI CD8a+ T cells (Figure 2C). Compared to their WT ECI T cell counterparts, allogeneic CD8a+ T cells expressed similar levels of *Cd69* but were enriched in transcripts for the integrin α4β7 and the cytotoxic T cell markers *Gzmb*, *Fasl* and *Ifng* (Figure 2D). In contrast, allogeneic CD8a+ T cells exhibited low expression of *Itgae* and *Ccr9*, which are typically expressed by T cells in the normal WT gut epithelial compartment (Figure 2D).

To verify that the qPCR results, which detect only partial cDNA fragments, reflected expression of the full-length *Glp1r* mRNA transcript in allogeneic ECI T cells, we performed conventional RT-PCR using primer pairs spanning the entire *Glp1r* open reading frame, followed by gel electrophoresis. As shown in Figure 2E, a 1.4-kb PCR

product, corresponding to the entire coding region of the canonical mouse *Glp1r*, was amplified from RNA obtained from 2 independent samples of sorted allogeneic ECI CD8a+ T cells.

We next assessed whether the allogeneic ECI T cell *Glp1r* mRNA encodes a functional protein by measuring cAMP induction in response to the GLP-1R agonist exendin-4 in gut ECI CD8a+ T cells sorted from WT C57BL/6 and WT BALB/c mice, as well as from BALB/c-into-C57BL/6 allogeneic mice. Consistent with previous findings using isolated IELs [12], Ex-4 (10 nM) directly increased cAMP levels in all three ECI sorted T cell groups (Figure 2F). Although the magnitude of induction was slightly lower in the CD8a+ T cells from the allogeneic group, the relative cAMP response triggered by the forskolin positive control was preserved and comparable in the three groups.

Loss-of-function experiments are an independent and complementary strategy to evaluate whether the absence of GLP-1R signaling within the T cells infiltrating the host GI tract influences the characteristics of aGvHD. To address this question in regard to the GLP-1R, we conducted a fully mismatched HCT using C57BL/6 WT (*Glp1r*$^{+/+}$) or C57BL/6 GLP-1R KO (*Glp1r*$^{-/-}$) mice as allogeneic donors into BALB/c recipients to induce aGvHD in the GI tract. As controls, syngeneic transplants were also performed using BALB/c donors to generate aGvHD-negative mice (Figure 3A).

When compared to BALB/c syngeneic mice, BALB/c recipients of C57BL/6 WT or C57BL/6 GLP-1R KO donor HCT experienced similar degrees of BW loss and marked upregulation of plasma cytokines associated with aGvHD progression (Figure 3B,C). Hence, C57BL/6 WT and C57BL/6 GLP-1R KO donor T cells exhibit the same allogeneic potential for induction of aGvHD. Allogeneic C57BL/6 WT and C57BL/6 GLP-1R KO chimerism was greater than 98% when assessed in PBMC (Figure 3D) and the ECI (Figure 3Ea). Within the ECI the percentage of allogeneic C57BL/6 CD3+CD8a+ T cells was equivalent in C57BL/6 WT and C57BL/6 GLP-1R KO mice (79% of the CD45+ events) (Figure 3Eb), however only a minor fraction corresponded to CD69+CD103+ T cells and that proportion was further reduced in C57BL/6 GLP-1R KO mice (Figure 3Ec and 3Ed).

To confirm the identity of allogeneic C57BL/6 WT and C57BL/6 GLP-1R KO donor immune cells isolated from the intestinal ECI of BALB/c recipient mice, we performed TaqMan gene expression assays targeting specific exon boundaries of the *Glp1r* transcript. In the whole body C57BL/6 GLP-1R KO mouse, disruption of the *Glp1r* gene results from the internal deletion of exons 6 and 7 within the *Glp1r* coding sequence [28,53]. Data in Figure 3F confirmed the expression of *Glp1r* exons 3−4 in RNA extracted from both C57BL/6 WT and C57BL/6 GLP-1R KO donor cells. As expected, exons 5−6, which are absent in C57BL/6 GLP-1R KO mouse tissues, were expressed in C57BL/6 WT cells. Interestingly, ∼8% contribution of *Glp1r* exons 5−6 signal was also detected in donor C57BL/6 GLP-1R KO ECI. This signal likely reflects the contribution of the residual 2% BALB/c host IEL T cells, which express a BALB/c WT *Glp1r*, to the donor C57BL/6 GLP-1R KO ECI. This interpretation aligns with the gut ECI chimerism data presented in Figure 3Ea.

The degree of mucosal damage in the ileum, assessed by counting Paneth cell numbers and crypt apoptotic bodies, was comparable in BALB/c mice receiving allogeneic HCT from either C57BL/6 WT or C57BL/6 GLP-1R KO donors, and was significantly greater than that observed in syngeneic controls (Figure 3G). Whereas mRNA levels of the ISC marker *Lgr5* were similar between syngeneic and allogeneic groups, expression of other epithelial lineage markers, particularly *Reg3g*, was consistently reduced to the same extent in both C57BL/6 WT and C57BL/6 GLP-1R KO allogeneic mice compared to syngeneic controls (Figure 3H). In agreement with the data shown in Figure 1H, *Glp1r* expression was elevated in the ileum of BALB/c recipients of C57BL/6 WT allogeneic HCT, but not in those receiving transplants from C57BL/6 GLP-1R KO donors (Figure 3I). This finding is consistent with the mRNA analysis of donor immune cells isolated from the intestinal ECI of BALB/c recipients (Figure 3F).

Studies in murine models of GvHD have identified two distinct phases of BW loss in allogeneic recipients: i) an initial, non-lethal phase occurring around days 5−10 post-HCT, followed by a recovery period, and ii) a second phase that progresses until death [54]. These phases correspond to two waves of donor CD8^{+} T cell expansion in allogeneic recipients [55]. To determine the potential dependence on GLP-1R signaling for the weight loss observed during aGvHD, we performed a BALB/c-into-C57BL/6 allogeneic HCT using either C57BL/6 WT or C57BL/6 GLP-1R KO recipients and monitored BW loss and survival throughout aGvHD progression (Figure 3J). Both C57BL/6 WT and C57BL/6 GLP-1R KO recipient mice exhibited nearly identical BW loss profiles up to day 20 (Figure 3K). Beyond this point, the small number of surviving mice limited the ability to accurately display BW trends. Survival analysis revealed no significant difference between C57BL/6 WT and C57BL/6 GLP-1R KO recipient mice, with a median survival of 22 days in both groups (Figure 3L).

Substantial evidence from preclinical and clinical studies implicates the gut microbiota in the pathophysiology of intestinal mucosal injury associated with aGvHD [56]. To explore how acute GvHD and GLP-1R signaling shape the gut microbial communities, we performed 16S rRNA sequencing. In the semaglutide experiments, neither alpha diversity, assessed by observed richness and Chao1 index, nor beta diversity, assessed by principal coordinate analysis (PCoA), differed significantly across groups (Figure 4A,B). Differential abundance analysis using DESeq2 identified two genera affected by semaglutide: *Massiliomicrobiota*, which was upregulated by aGvHD but suppressed

Figure 2: A functional GLP-1R is expressed by the allogeneic T cells homing to the gut during aGvHD. **(A)** C57BL/6 (C57) mice underwent HCT from allogeneic (Allo) BALB/c (B/c) donors. Small intestine immune cells from the conjoined intestinal lamina propria, submucosa and muscle layers (LPM) and ECI were isolated 9 days and 10 days, respectively, after HCT, stained and subjected to FACS, followed by RNA analysis and cAMP production assays. **(B)** Dot plots representing the gating strategy used for sorting normal wild-type (WT) C57BL/6 intestinal ECI T cells and allogeneic T cells isolated from the gut ECI and LPM compartments. **(C)** *Glp1r* mRNA expression levels in the sorted cell samples shown in panel (B), and **(D)** gene expression profile of T cells sorted from WT and allogeneic ECI. mRNA levels are mean ± SD from two independent experiments, each involving pooled sorted cells from n = 3−4 mice. **(E)** *Glp1r* and *Gapdh* mRNA expression were assessed by RT-PCR in total RNA from WT C57BL/6 mouse Percoll-purified (PP) gut ECI and from sorted allogeneic intestinal ECI CD3+CD8a+ T cells. PCR products were analyzed by agarose gel electrophoresis followed by SYBR Green staining. The specificity of each RT reaction (+) was monitored by control reactions using samples in which reverse transcriptase was omitted from the RT reaction mixture (−). The top arrow indicates a single PCR product (1410 bp long) encompassing the majority of the *Glp1r* open reading frame. **(F)** cAMP levels in small intestine ECI sorted CD3+CD8a+ T cells from WT C57BL/6, WT BALB/c, and BALB/c-into-C57BL/6 allogeneic mice. The sorted cells were challenged for 15 min with vehicle (Veh), exendin-4 (Ex4), or forskolin (Fk) at the indicated concentrations. To facilitate comparison, the data are normalized to the specific Veh-treated cAMP levels from each of the three sources of sorted cells. Data are mean ± SD from 2 to 4 replicates from pooled cells from n = 6 WT C57BL/6, 6 WT BALB/c, and 6 allogeneic mice. *$p \leq 0.05$ and ****$p \leq 0.0001$ by 1- or 2-way ANOVA followed by Dunnett's test with Veh as the control.

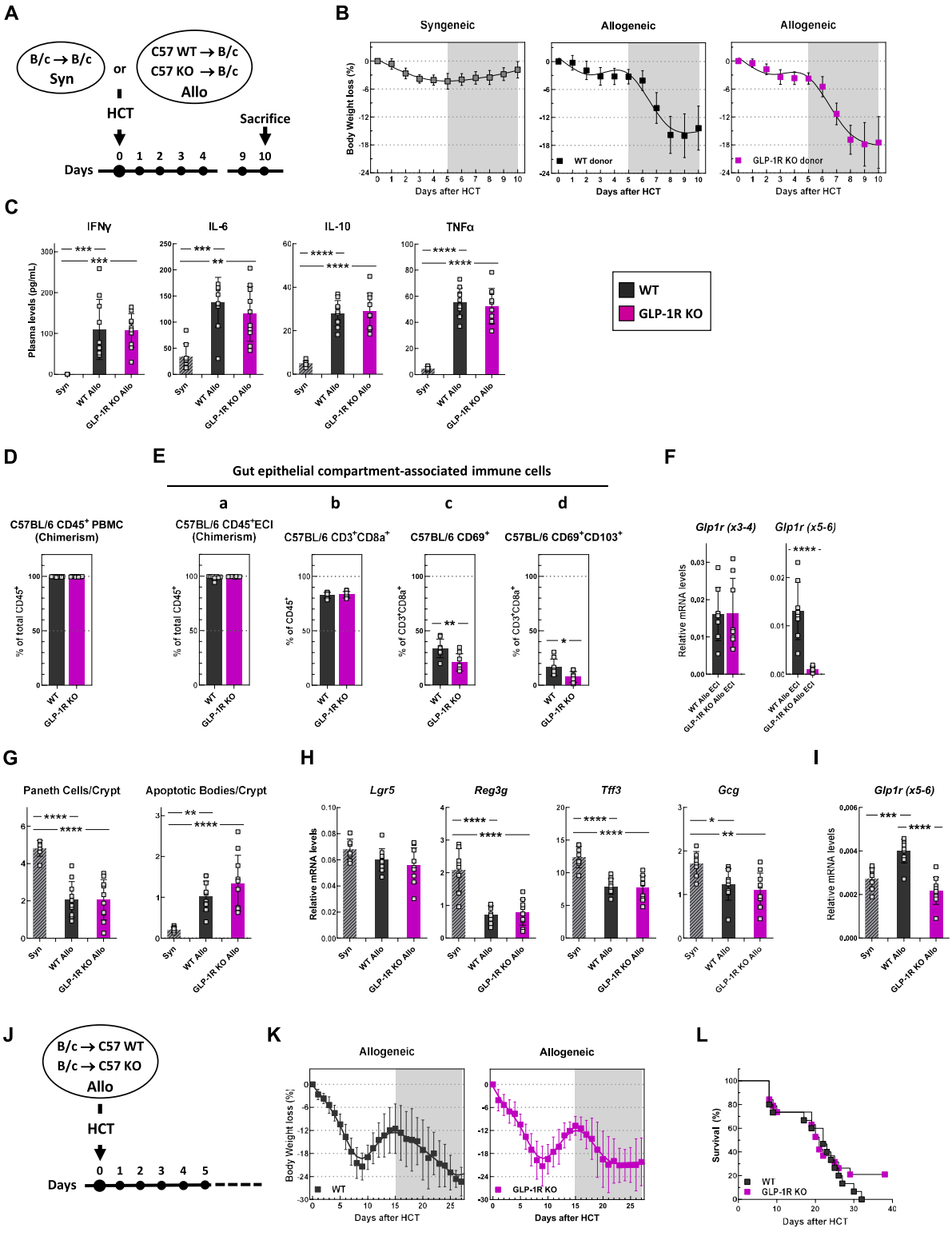

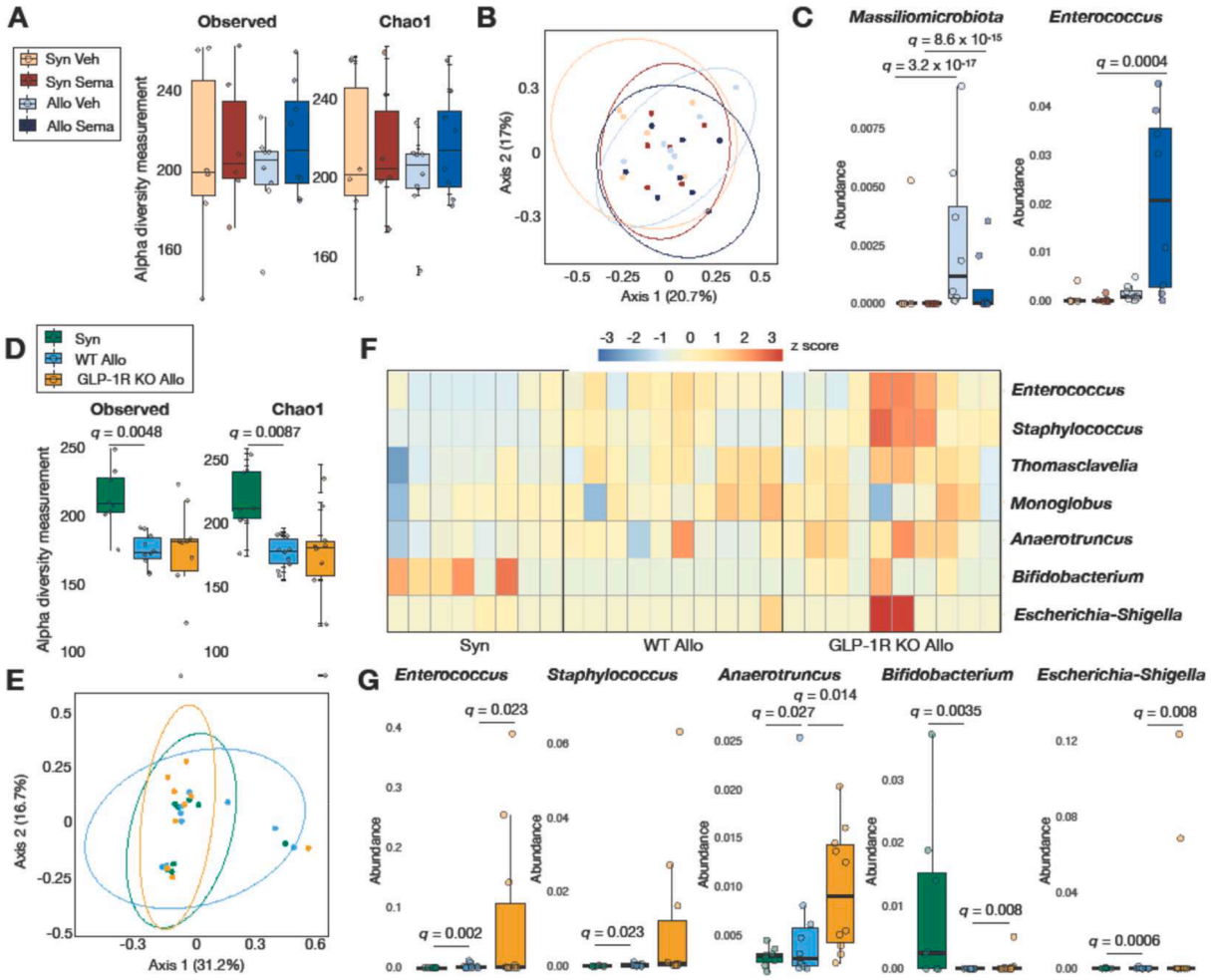

Figure 4: GLP-1R signaling modulates specific gut microbiota taxa during aGvHD. (**A**) Alpha diversity (Observed and Chao1 indices) of gut microbiota in C57BL/6 mice receiving HCT from C57BL/6 donors (Syn) or BALB/c donors (Allo) treated with vehicle (Veh) or semaglutide (Sema) 6 days prior to HCT until the time of sacrifice. (**B**) Principal Coordinates Analysis (PCoA) of Bray–Curtis dissimilarity of microbiota profiles from the mice in (**A**). (**C**) Relative abundance of *Massiliomicrobiota* and *Enterococcus* was significantly altered between vehicle-treated allogeneic and syngeneic groups and modulated by semaglutide treatment. (**D**) Alpha diversity of gut microbiota in BALB/c mice receiving HCT from BALB/c donors (Syn), C57BL/6 WT donors (WT Allo), or C57BL/6 GLP-1R KO donors (GLP-1R KO Allo). (**E**) PCoA of Bray–Curtis dissimilarity showing similar clustering of microbiota profiles from recipient mice in (**D**). (**F**) Heatmap of z-score normalized relative abundance of top differentially abundant genera across recipient groups in (**D**). (**G**) Relative abundance of *Enterococcus*, *Staphylococcus*, *Anaerotruncus*, *Bifidobacterium*, and *Escherichia-Shigella* were significantly altered. Statistical significance was determined by Kruskal–Wallis test with false discovery rate correction in **D**, and by DESeq2 with multiple testing correction in **C** and **G**.

by semaglutide, and *Enterococcus*, which was further enriched in semaglutide-treated allogeneic recipients (Figure 4C).

In BALB/c recipients of syngeneic BALB/c, allogeneic C57BL/6 WT, or allogeneic C57BL/6 GLP-1R KO cells, alpha diversity was significantly reduced in allogeneic mice receiving C57BL/6 WT cells. A similar trend was observed in those receiving C57BL/6 GLP-1R KO cells, although the reduction did not reach statistical significance relative to syngeneic controls (Figure 4D). Beta diversity analysis showed substantial overlap in microbiota composition across all groups (Figure 4E). Despite this, DESeq2-based analysis identified five microbial genera, including *Enterococcus*, *Staphylococcus*, *Thomsclavelia*, *Monoglobus*, and *Anaerotruncus*, that were consistently

Figure 3: Genetic ablation studies indicate that loss of GLP-1R signaling in either donor or recipient mice undergoing allogeneic HCT does not impact aGvHD severity or survival. (A) Schematic of the experimental design. BALB/c (B/c) mice underwent HCT from syngeneic (Syn) BALB/c donors (n = 8) or allogeneic (Allo) C57BL/6 WT (C57 WT) (n = 10) or C57BL/6 GLP-1R KO (C57 KO) (n = 10) donors. (**B**) Sequence of body weight loss during the experiment. The grey shaded area is a visual reference to compare the body weight decline in the allogeneic mice relative to the syngeneic group indicative of aGvHD progress. (**C**) Plasma cytokine levels. (**D** and **E**) Chimerism assessed at the time of sacrifice by flow cytometry on (**D**) PBMC and (**E**) small intestine ECI isolated from allogeneic BALB/c recipient mice. (**F**) mRNA expression of *Glp1r* measured by qPCR in gut ECI of allogeneic BALB/c recipients (n = 8). (**G**) Number of Paneth cells and apoptotic bodies per crypt in ileal tissue. (**H**) mRNA expression of select epithelial cell lineage markers and (**I**) *Glp1r* in ileum measured by qPCR. Data from panels B to I are mean ± SD pooled from 2 independent experiments comprising mice from the same cohort. $*p \leq 0.05$, $**p \leq 0.01$, $***p \leq 0.001$ and $****p \leq 0.0001$ by Student's t tests (panels **E** and **F**) and by 1-way ANOVA followed by Tukey's multiple comparisons tests (panels **C** and **G** to **I**). (**J**) C57BL/6 WT (n = 15) and C57BL/6 GLP-1R KO (n = 20) mice underwent HCT from allogeneic BALB/c donors. (**K**) Sequence of body weight loss during the experiment. The grey shaded area is a visual reference to compare the body weight decline in the allogeneic mice during the lethal phase of the aGvHD. Data are mean ± SD. (**L**) Kaplan–Meier survival plots of C57BL/6 WT and C57BL/6 GLP1-R KO allogeneic mice. Survival curves compared using the Log-rank (Mantel–Cox) test showed no significant difference. Panels **K** and **L** are data combined from 2 independent experiments comprising mice from the same cohort.

enriched in allogeneic recipients (Figure 4F). Notably, *Bifidobacterium* and *Escherichia-Shigella* were significantly depleted in allogeneic mice receiving C57BL/6 WT cells compared to syngeneic controls. In contrast, recipients of C57BL/6 GLP-1R KO donor cells exhibited increased levels of *Enterococcus*, *Staphylococcus*, *Anaerotruncus*, and *Escherichia-Shigella*, along with reduced *Bifidobacterium* (Figure 4G), suggesting a partial shift in microbiota composition influenced by GLP-1R signaling. Biomarker identification using LEfSe and functional predictions using PICRUSt2 did not reveal significant changes in microbial metabolic pathways in either model. Together, these data suggest that while GLP-1R signaling has limited effects on overall microbial diversity during acute GvHD, it exerts selective pressure on key microbial taxa such as *Enterococcus*.

4. DISCUSSION

The IEL is the major immune cell type that expresses the GLP-1R. Recent studies have expanded the physiological importance of the IEL GLP-1R for the control of local immune responses by using genetic targeting to selectively ablate the *Glp1r* in gut mucosal T cells. Notably, the gut IEL GLP-1R is required for the actions of GLP-1 medicines to attenuate both local and systemic T cell-induced inflammation, but is dispensable for the GLP-1R-dependent reduction of lipopolysaccharide-induced inflammation [11]. These local anti-inflammatory actions are mediated through canonical GLP-1R signaling linking protein kinase A activity to reduction of proximal T cell receptor signaling. Consistent with the local anti-inflammatory actions exerted through populations of GLP-1R+ IELs, blockade of GLP-1R signaling using the GLP-1R antagonist exendin(9—39) augments T cell activity and anti-tumor immunity in a mouse model of colorectal cancer [21].

As the actions of GLP-1 in the gut encompass augmentation of mucosal defense, together with attenuation of experimental and clinical inflammation in part through reduction of gut T cell activity [25], we hypothesized that GLP-1RAs, exemplified by semaglutide, might reduce the severity of gastrointestinal injury, a hallmark of acute and chronic GvHD known to be predominantly driven by T cells. Consistent with data shown in Figure 1, the experimental paradigm studied here closely recapitulates key pathological features of aGvHD in our BALB/c-into-C57BL/6 allogeneic murine model, displaying progressive weight loss, marked upregulation of circulating cytokines, recruitment of allogeneic T cells into the intestinal crypts, mucosal injury in the gut and suppression of the ileal antimicrobial aGvHD biomarker *Reg3g*.

Although our analyses demonstrated the presence of functional GLP-1Rs on the allogeneic T cells infiltrating the GI tract during aGvHD (Figure 2), chronic activation of the GLP-1R via semaglutide administration failed to attenuate the clinical course of aGvHD. Nevertheless, at the dose used here, semaglutide exerts sufficient engagement of the GLP-1R to improve glucose homeostasis and reduce inflammation and atherosclerosis, with only modest reduction of body weight [31,32]. Complementary genetic ablation studies (Figure 3) further demonstrated that loss of GLP-1R signaling by the allogeneic donor T cells did not impact disease severity or recipient survival, collectively indicating that both pharmacological GLP-1R activation and loss of endogenous GLP-1R signalling are both dispensable for immunopathogenesis of murine aGvHD modeled herein.

Over the past decade, the commensal microbiota and their derivatives (pathogen-associated molecular patterns (PAMPs) and metabolites) have emerged as key modulators of GvHD. Following allogeneic HCT, the ensuing intestinal inflammation is associated with major shifts in microbiota composition and marked loss of gut microbiota physiological diversity [56]. These disruptions can, in turn, contribute to the severity of intestinal inflammation and the progression of GvHD. Our analysis of microbiota in mice with aGvHD revealed modest differences in the proportions of *Enterococcus*, *Staphylococcus*, *Thomsclavelia*, *Monoglobus*, and *Anaerotruncus* as well as upregulation of *Enterococci* and downregulation of *Massiliomicrobiota* in response to semaglutide administration. Nevertheless, given the overall findings that gain or loss of GLP-1R signaling does not meaningfully modify outcomes in aGvHD, the significance of these changes in microbiota representation remains uncertain.

The anti-inflammatory actions of GLP-1 medicines, mediated in part through direct effects on T cells, including IELs, and through inter-organ communication involving neuronal GLP-1R signaling, are gaining increasing attention in diseases characterized by dysregulated inflammation [11,12,21,31,57]. In clinical settings, C-reactive protein levels are frequently reduced in patients treated with GLP-1 medicines, supporting their anti-inflammatory potential. However, because GLP-1 medicines often induce weight loss, it can be challenging to distinguish weight loss-independent mechanisms underlying these anti-inflammatory effects. Nonetheless, weight loss-independent actions of GLP-1 medicines have also been described in humans [25,58,59]. Our preclinical studies using a model scrutinizing the putative role of GLP-1R+ gut T cells, a major immune population expressing the GLP-1R, provide evidence that GLP-1 medicines are not uniformly anti-inflammatory, and that their inherent ability to reduce systemic inflammation and intestinal injury is highly context-dependent.

4.1. Limitations

Our study focused exclusively on an MHC-mismatched murine model of aGvHD. While this system recapitulates the rapid onset and high severity typical of clinical aGvHD, it does not encompass the more gradual disease kinetics or subtler immune interactions seen in minor histocompatibility antigen (miHA)-mismatched transplantation settings. The single mouse model used here may underestimate therapeutic efficacy under high-inflammation conditions. We used male mice, and the potential importance of sex in determining roles for GLP-1R signaling in aGvHD was not examined. Finally, the doses of semaglutide used here, chosen to minimize weight loss, as well as the timing and duration of exposure, may be insufficient to capture the therapeutic potential of GLP-1 medicines in aGvHD.

While our study has primarily focused on the GI tract, recognized as the principal initial target organ in aGvHD, it is important to acknowledge that aGvHD can also affect other organs. These include classical target sites such as the liver, lungs, and skin, as well as potential non-classical targets like the kidneys, bone marrow, and central nervous system, which were not examined in our current analyses.

ACKNOWLEDGMENTS

DJD is supported by a Banting and Best Diabetes Centre Novo Nordisk Chair in Incretin Biology, a Sinai Health-Novo Nordisk Foundation Chair in Regulatory Peptides, CIHR grants 154321 and 192044 and Diabetes Canada-Canadian Cancer Society Grant OG-3- 24-5819-DD.

CRediT AUTHORSHIP CONTRIBUTION STATEMENT

Bernardo Yusta: Writing — review & editing, Writing — original draft, Project administration, Methodology, Investigation, Formal analysis, Data curation, Conceptualization. **Chi Kin Wong:** Writing — review &

editing, Writing — original draft, Formal analysis. **Dianne Matthews:** Writing — review & editing, Investigation, Formal analysis. **Jacqueline A. Koehler:** Writing — review & editing, Writing — original draft, Investigation, Formal analysis, Conceptualization. **Laurie L. Baggio:** Writing — review & editing, Writing — original draft, Investigation, Formal analysis, Conceptualization. **KW Annie Bang:** Writing — review & editing, Writing — original draft, Methodology, Investigation, Formal analysis. **Daniel J. Drucker:** Writing — review & editing, Writing — original draft, Supervision, Methodology, Funding acquisition, Formal analysis, Data curation, Conceptualization.

DECLARATION OF COMPETING INTEREST

The authors declare the following financial interests/personal relationships which may be considered as potential competing interests: Drucker reports a relationship with Anylam, Amgen, AstraZeneca Inc., Crinetics, Eli Lilly, Insulet, Kallyope, Metsara, and Pfizer Inc. that includes: consulting or advisory. Mount Sinai Hospital, has received investigator-initiated grant support from Amgen, Eli Lilly Inc., Novo Nordisk, Pfizer and Zealand Pharmaceuticals Inc. to support preclinical studies in the Drucker laboratory. If there are other authors, they declare that they have no known competing financial interests or personal relationships that could have appeared to influence the work reported in this paper.

DATA AVAILABILITY

Data will be made available on request.

APPENDIX A. SUPPLEMENTARY DATA

Supplementary data to this article can be found online at https://doi.org/10.1016/j.molmet.2025.102235.

REFERENCES

[1] Drucker DJ, Holst JJ. The expanding incretin universe: from basic biology to clinical translation. Diabetologia 2023;66(10):1765—79.

[2] Drucker DJ, Yusta B. Physiology and pharmacology of the enteroendocrine hormone glucagon-like peptide-2. Annu Rev Physiol 2014;76:561—83.

[3] Drucker DJ, Habener JF, Holst JJ. Discovery, characterization, and clinical development of the glucagon-like peptides. J Clin Investig 2017;127(12):4217—27.

[4] McLean BA, Wong CK, Campbell JE, Hodson DJ, Trapp S, Drucker DJ. Revisiting the complexity of GLP-1 action from sites of synthesis to receptor activation. Endocr Rev 2021;42(2):101—32.

[5] Kahles F, Meyer C, Mollmann J, Diebold S, Findeisen HM, Lebherz C, et al. GLP-1 secretion is increased by inflammatory stimuli in an IL-6-dependent manner, leading to hyperinsulinemia and blood glucose lowering. Diabetes 2014;63(10):3221—9.

[6] Ellingsgaard H, Hauselmann I, Schuler B, Habib AM, Baggio LL, Meier DT, et al. Interleukin-6 enhances insulin secretion by increasing glucagon-like peptide-1 secretion from L cells and alpha cells. Nat Med 2011;17(11):1481—9.

[7] Lebrun LJ, Lenaerts K, Kiers D, Pais de Barros JP, Le Guern N, Plesnik J, et al. Enteroendocrine L cells sense LPS after gut barrier injury to enhance GLP-1 secretion. Cell Rep 2017;21(5):1160—8.

[8] Nguyen AT, Mandard S, Dray C, Deckert V, Valet P, Besnard P, et al. Lipopolysaccharides-mediated increase in glucose-stimulated insulin secretion: involvement of the GLP-1 pathway. Diabetes 2014;63(2):471—82.

[9] Koehler JA, Baggio LL, Yusta B, Longuet C, Rowland KJ, Cao X, et al. GLP-1R agonists promote normal and neoplastic intestinal growth through mechanisms requiring Fgf7. Cell Metab 2015;21(3):379—91.

[10] Simonsen L, Pilgaard S, Orskov C, Rosenkilde MM, Hartmann B, Holst JJ, et al. Exendin-4, but not dipeptidyl peptidase IV inhibition, increases small intestinal mass in GK rats. Am J Physiol Gastrointest Liver Physiol 2007;293(1):G288—95.

[11] Wong CK, Yusta B, Koehler JA, Baggio LL, McLean BA, Matthews D, et al. Divergent roles for the gut intraepithelial lymphocyte GLP-1R in control of metabolism, microbiota, and T cell-induced inflammation. Cell Metab 2022;34(10):1514—1531 e1517.

[12] Yusta B, Baggio LL, Koehler J, Holland D, Cao X, Pinnell LJ, et al. GLP-1 receptor (GLP-1R) agonists modulate enteric immune responses through the intestinal intraepithelial lymphocyte (IEL) GLP-1R. Diabetes 2015;64(7):2537—49.

[13] Bang-Berthelsen CH, Holm TL, Pyke C, Simonsen L, Sokilde R, Pociot F, et al. GLP-1 induces barrier protective expression in brunner's glands and regulates colonic inflammation. Inflamm Bowel Dis 2016;22(9):2078—97.

[14] Wang W, Zhang C, Zhang H, Li L, Fan T, Jin Z. The alleviating effect and mechanism of GLP-1 on ulcerative colitis. Aging (Albany NY) 2023;15(16):8044—60.

[15] Sun H, Shu J, Tang J, Li Y, Qiu J, Ding Z, et al. GLP-1 receptor agonists alleviate colonic inflammation by modulating intestinal microbiota and the function of group 3 innate lymphoid cells. Immunology 2024;172(3):451—68.

[16] Kissow H, Viby NE, Hartmann B, Holst JJ, Timm M, Thim L, et al. Exogenous glucagon-like peptide-2 (GLP-2) prevents chemotherapy-induced mucositis in rat small intestine. Cancer Chemother Pharmacol 2012;70(1):39—48.

[17] Brubaker PL. Glucagon-like Peptide-2 and the regulation of intestinal growth and function. Compr Physiol 2018;8(3):1185—210.

[18] Nozu T, Miyagishi S, Kumei S, Nozu R, Takakusaki K, Okumura T. Glucagon-like peptide-1 analog, liraglutide, improves visceral sensation and gut permeability in rats. J Gastroenterol Hepatol 2018;33(1):232—9.

[19] Su Y, Liu N, Zhang Z, Li H, Ma J, Yuan Y, et al. Cholecystokinin and glucagon-like peptide-1 analogues regulate intestinal tight junction, inflammation, dopaminergic neurons and alpha-synuclein accumulation in the Colon of two parkinson's disease mouse models. Eur J Pharmacol 2022;926:175029.

[20] Voetmann LM, Underwood CR, Rolin B, Hansen AK, Kirk RK, Pyke C, et al. In vitro cell cultures of Brunner's glands from male mouse to study GLP-1 receptor function. Am J Physiol Cell Physiol 2022;322(6):C1260—9.

[21] Ben Nasr M, Usuelli V, Dellepiane S, Seelam AJ, Fiorentino TV, D'Addio F, et al. Glucagon-like peptide 1 receptor is a T cell-negative costimulatory molecule. Cell Metab 2024;36(6):1302—1319 e1312.

[22] Wang Z, Wang M, Hu X, Li Y, Ma D, Li S, et al. Liraglutide, a glucagon-like Peptide-1 receptor agonist, attenuates development of cardiac Allograft vasculopathy in a murine heart transplant model. Transplantation 2019;103(3):502—11.

[23] Peng L, Lai W, Yu S, Li Q, Jiang X, Chen G. GLP-1 and glucagon receptor dual agonism ameliorates kidney allograft fibrosis by improving lipid metabolism. Front Immunol 2025;16:1551136.

[24] Mehdi SF, Pusapati S, Anwar MS, Lohana D, Kumar P, Nandula SA, et al. Glucagon-like peptide-1: a multi-faceted anti-inflammatory agent. Front Immunol 2023;14:1148209.

[25] Drucker DJ. The benefits of GLP-1 drugs beyond obesity. Science 2024;385(6706):258—60.

[26] Ebbesen M, Kissow H, Hartmann B, Kielsen K, Sorensen K, Stinson SE, et al. Glucagon-like Peptide-1 is associated with systemic inflammation in pediatric patients treated with hematopoietic stem cell transplantation. Front Immunol 2021;12:793588.

[27] Sorum ME, Gang AO, Tholstrup DM, Gudbrandsdottir S, Kissow H, Kornblit B, et al. Semaglutide treatment for PRevention of toxicity in high-dosE chemotherapy with autologous haematopoietic stem-cell transplantation (PROTECT): study protocol for a randomised, double-blind, placebo-controlled, investigator-initiated study. BMJ Open 2024;14(10):e089862.

[28] Scrocchi LA, Brown TJ, MaClusky N, Brubaker PL, Auerbach AB, Joyner AL, et al. Glucose intolerance but normal satiety in mice with a null mutation in the glucagon-like peptide 1 receptor gene. Nat Med 1996;2(11):1254–8.
[29] Pujadas G, Varin EM, Baggio LL, Mulvihill EE, Bang KWA, Koehler JA, et al. The gut hormone receptor GIPR links energy availability to the control of hematopoiesis. Mol Metabol 2020;39:101008.
[30] Hammoud R, Kaur KD, Koehler JA, Baggio LL, Wong CK, Advani KE, et al. Glucose-dependent insulinotropic polypeptide receptor signaling alleviates gut inflammation in mice. JCI Insight 2024;10(3).
[31] McLean BA, Wong CK, Kaur KD, Seeley RJ, Drucker DJ. Differential importance of endothelial and hematopoietic cell GLP-1Rs for cardiometabolic versus hepatic actions of semaglutide. JCI Insight 2021;6(22).
[32] Rakipovski G, Rolin B, Nohr J, Klewe I, Frederiksen KS, Augustin R, et al. The GLP-1 analogs liraglutide and semaglutide reduce atherosclerosis in ApoE(-/-) and LDLr(-/-) mice by a mechanism that includes inflammatory pathways. JACC Basic Transl Sci 2018;3(6):844–57.
[33] Goodyear AW, Kumar A, Dow S, Ryan EP. Optimization of murine small intestine leukocyte isolation for global immune phenotype analysis. J Immunol Methods 2014;405:97–108.
[34] Panjwani N, Mulvihill EE, Longuet C, Yusta B, Campbell JE, Brown TJ, et al. GLP-1 receptor activation indirectly reduces hepatic lipid accumulation but does not attenuate development of atherosclerosis in diabetic Male ApoE-/- mice. Endocrinology 2013;154(1):127–39.
[35] Fuchs S, Yusta B, Baggio LL, Varin EM, Matthews D, Drucker DJ. Loss of Glp2r signaling activates hepatic stellate cells and exacerbates diet-induced steatohepatitis in mice. JCI Insight 2020;5(8).
[36] Callahan BJ, McMurdie PJ, Rosen MJ, Han AW, Johnson AJ, Holmes SP. DADA2: high-resolution sample inference from Illumina amplicon data. Nat Methods 2016;13(7):581–3.
[37] McMurdie PJ, Holmes S. Phyloseq: an R package for reproducible interactive analysis and graphics of microbiome census data. PLoS One 2013;8(4):e61217.
[38] Love MI, Huber W, Anders S. Moderated estimation of fold change and dispersion for RNA-seq data with DESeq2. Genome Biol 2014;15(12):550.
[39] Segata N, Izard J, Waldron L, Gevers D, Miropolsky L, Garrett WS, et al. Metagenomic biomarker discovery and explanation. Genome Biol 2011;12(6). R60.
[40] Douglas GM, Maffei VJ, Zaneveld JR, Yurgel SN, Brown JR, Taylor CM, et al. PICRUSt2 for prediction of metagenome functions. Nat Biotechnol 2020;38(6):685–8.
[41] Fu YY, Egorova A, Sobieski C, Kuttiyara J, Calafiore M, Takashima S, et al. T cell recruitment to the intestinal stem cell compartment drives immune-mediated intestinal damage after allogeneic transplantation. Immunity 2019;51(1):90–103 e103.
[42] Takashima S, Martin ML, Jansen SA, Fu Y, Bos J, Chandra D, et al. T cell-derived interferon-gamma programs stem cell death in immune-mediated intestinal damage. Sci Immunol 2019;4(42).
[43] Hill GR, Crawford JM, Cooke KR, Brinson YS, Pan L, Ferrara JL. Total body irradiation and acute graft-versus-host disease: the role of gastrointestinal damage and inflammatory cytokines. Blood 1997;90(8):3204–13.
[44] Hill GR, Koyama M. Cytokines and costimulation in acute graft-versus-host disease. Blood 2020;136(4):418–28.
[45] Fajgenbaum DC, June CH. Cytokine storm. N Engl J Med 2020;383(23):2255–73.
[46] Deeg HJ, Storb R. Acute and chronic graft-versus-host disease: clinical manifestations, prophylaxis, and treatment. J Natl Cancer Inst 1986;76(6):1325–8.
[47] Nikolic B, Lee S, Bronson RT, Grusby MJ, Sykes M. Th1 and Th2 mediate acute graft-versus-host disease, each with distinct end-organ targets. J Clin Investig 2000;105(9):1289–98.
[48] Kok L, Masopust D, Schumacher TN. The precursors of CD8(+) tissue resident memory T cells: from lymphoid organs to infected tissues. Nat Rev Immunol 2022;22(5):283–93.
[49] Teshima T, Reddy P, Zeiser R. Acute graft-versus-host disease: novel biological insights. Biol Blood Marrow Transplant 2016;22(1):11–6.
[50] Zhao D, Kim YH, Jeong S, Greenson JK, Chaudhry MS, Hoepting M, et al. Survival signal REG3alpha prevents crypt apoptosis to control acute gastrointestinal graft-versus-host disease. J Clin Investig 2018;128(11):4970–9.
[51] McDonagh SC, Lee J, Izzo A, Brubaker PL. Role of glial cell-line derived neurotropic factor family receptor alpha2 in the actions of the glucagon-like peptides on the murine intestine. Am J Physiol Gastrointest Liver Physiol 2007;293(2):G461–8.
[52] Varin EM, Mulvihill EE, Baggio LL, Koehler JA, Cao X, Seeley RJ, et al. Distinct neural sites of GLP-1R expression mediate physiological versus pharmacological control of incretin action. Cell Rep 2019;27(11):3371–3384 e3373.
[53] Flamez D, Van Breuseghem A, Scrocchi LA, Quartier E, Pipeleers D, Drucker DJ, et al. Mouse pancreatic beta cells exhibit preserved glucose competence after disruption of the glucagon-like peptide 1 receptor gene. Diabetes 1998;47:646–52.
[54] van Leeuwen L, Guiffre A, Atkinson K, Rainer SP, Sewell WA. A two-phase pathogenesis of graft-versus-host disease in mice. Bone Marrow Transplant 2002;29(2):151–8.
[55] Li X, Deng R, He W, Liu C, Wang M, Young J, et al. Loss of B7-H1 expression by recipient parenchymal cells leads to expansion of infiltrating donor CD8+ T cells and persistence of graft-versus-host disease. J Immunol 2012;188(2):724–34.
[56] Fredricks DN. The gut microbiota and graft-versus-host disease. J Clin Investig 2019;129(5):1808–17.
[57] Wong CK, McLean BA, Baggio LL, Koehler JA, Hammoud R, Rittig N, et al. Central glucagon-like peptide 1 receptor activation inhibits toll-like receptor agonist-induced inflammation. Cell Metab 2024;36(1):130–143 e135.
[58] Verma S, Petrie MC, Borlaug BA, Butler J, Davies MJ, Kitzman DW, et al. Inflammation in obesity-related HFpEF: the STEP-HFpEF program. J Am Coll Cardiol 2024;84(17):1646–62.
[59] Rodbard HW, Rosenstock J, Canani LH, Deerochanawong C, Gumprecht J, Lindberg SO, et al. Oral semaglutide versus empagliflozin in patients with type 2 diabetes uncontrolled on metformin: the PIONEER 2 trial. Diabetes Care 2019;42(12):2272–81.

